ELSEVIER

Marine and Petroleum Geology 19 (2002) 847–859

Marine and Petroleum Geology

www.elsevier.com/locate/marpetgeo

Individual characterization of petroleum fluid inclusions (composition and $P-T$ trapping conditions) by microthermometry and confocal laser scanning microscopy: inferences from applied thermodynamics of oils

R. Thiéry[a,*], J. Pironon[b], F. Walgenwitz[c], F. Montel[c]

[a]*UMR 6524 'Magmas et Volcans', Université Blaise Pascal, 5, rue Kessler, F-63038 Clermont-Ferrand Cedex, France*
[b]*UMR 7566 'G2R', Université Henri Poincaré, BP 23, F-54501 Vandoeuvre-les-Nancy, France*
[c]*Centre scientifique et technique Jean Feger, Avenue Larribau, F-64018 Pau, France*

Received 19 July 2002; received in revised form 30 September 2002; accepted 3 October 2002

Abstract

This paper proposes a new method to characterize individual oil-bearing fluid inclusions. It uses both the homogenisation temperatures measured by microthermometry, and the degree of gas bubble filling measured by confocal laser scanning microscopy, in conjunction with thermodynamic modelling for describing liquid–gas phase transitions and the volumetric behaviour of hydrocarbon mixtures. It is associated with a two-parameter (α, β) compositional model that describes the wide range of compositions of petroleums. We show that this method can give (1) useful estimations of the compositions and pressure–temperature entrapment conditions of oils in fluid inclusions, and (2) insights into the various processes that have affected these fluids either before entrapment (liquid–gas unmixing, gas leaching, mixing, etc.) or after (leakage, etc.).

Keywords: Fluid inclusions; Petroleum; Oil; Thermodynamic modelling

1. Introduction

Petroleum reservoir sandstones often contain aliquots of the oils that have migrated, and trapped as fluid inclusions. Thus, petroleum fluid inclusions are valuable objects that can give us important information about the composition, past migration processes and pressure–temperature conditions of the trapping of petroleum in sedimentary basins (Bodnar, 1990; Horsfield & McLimans, 1984; Isaksen, Pottorf, & Jenssen, 1998; Jensenius & Burruss, 1990; Karlsen, Nedkvitne, Larter, & Bjørlykke, 1993; Munz, Johansen, Holm, & Lacharpagne, 1999; Narr & Burruss, 1984; Pagel, Walgenwitz, & Dubessy, 1986). Accordingly, fluid inclusionists perform conventional microthermometry in order to determine the phase envelopes and the isochores of the inclusion fluids. This step of *PVT* modelling is the basis for interpreting microthermometric studies (Roedder, 1984) and requires the use of appropriate equations of state. It is most successful (Goldstein & Reynolds, 1994; Roedder, 1984) for simple fluids containing few components (CO_2, CH_4, H_2O,…), whose composition can be easily constrained by analytic procedures (Raman microspectrometry, etc.), but the situation is much more problematical for petroleum. Petroleums are complex fluids, which have many degrees of freedom, and a correspondingly large number of input parameters should theoretically be required to determine a trapping pressure. Thus, present research is trying to develop analytical techniques to get more accurate compositional data from fluid inclusions and better constrain PVT modelling. Crushing followed by gas chromatography coupled with mass spectrometry (Bratus, Svoren, & Danysh, 1975; Burruss, 1987; George, Ruble, Dutkiewicz, & Eadington, 2001; Horsfield & McLimans, 1984; Murray, 1957) or high performance liquid chromatography (Pang, George, & Quezada, 1998) are techniques which can be applied to bulk populations of fluid inclusions and can give accurate compositional data, but they do not take into account different inclusion generations trapped in one sample. Moreover, these bulk methods need perfect cleaning of the crushed sample to avoid contamination. Other analytical techniques, such as FT-IR spectroscopy (Pironon & Barrès, 1990, 1992), UV fluorescence-excitation emission spectroscopy (Kihle, 1996), UV-epifluorescence

* Corresponding author. Fax: +33-0473346744.
E-mail address: r.thiery@opgc.univ-bpclermont.fr (R. Thiéry).

0264-8172/02/$ - see front matter © 2002 Elsevier Science Ltd. All rights reserved.
PII: S0264-8172(02)00110-1

(Bodnar, 1990; Guilhaumou, Szydlowskii, & Pradier, 1990) have also been used to study petroleum fluid inclusions, but the measurements do not characterize the composition in sufficient detail for PVT modelling. Laser micropyrolysis coupled with gas chromatography–mass spectrometry (LPGC–MS) should provide chemical characterisation of individual inclusions (Greenwood, George, & Hall, 1998), but this technique is still at a developmental stage. Confocal scanning laser microscopy (CSLM), which is based on the fluorescence of liquid oil, permits the accurate measurement of the volume of the liquid phase of petroleum inclusions (Aplin et al., 1999; Mcleod, Larter, Aplin, Pedersen, & Booth, 1996; Pironon, Canals, Dubessy, Walgenwitz, & Laplace-Builhe, 1998).

The degree of gaseous filling (F_v) is an important parameter in PVT estimation, derived from the volume of the liquid phase and from the volume of the gas bubble, approximated to a sphere and measured by optical microscope. F_v can be measured at any temperature below the homogenisation temperature (T_h) (Fig. 1(a)). The accuracy of such measurement is around ±5%. The high resolution of CSLM (0.1 μm in x or y axis, 0.3 μm in z axis) allows us to estimate volumes for very tiny inclusions (>3 μm). In addition when solid precipitates occur in inclusions, they can be taken into account in the bulk volume estimate if they emit fluorescence. F_v is different at each point of the two-phase field of a P–T diagram. For a given P–T coordinate F_v will be different for different petroleum compositions. Thus, F_v measurements can be applied in association with microthermometry to provide additional constraints for estimating the compositions and pressure–temperature trapping conditions of petroleum fluid inclusions. However, the exploitation of these sets of microthermometric and volumetric data require integration with thermodynamic modelling. One method which achieves this, and is incorporated in the VTFlinc software (1997), has been proposed by the CALSEP society and the Newcastle Research Group (Aplin et al., 1999). This paper proposes an alternative approach, that has, we believe, some advantages over VTFlinc. Firstly, we describe the thermodynamic and compositional models for natural petroleums that are able to represent the PVT properties of petroleums. Next, we show how the method can be used to infer entrapment (P_{trap}–T_{trap}) values from (T_h–F_v) data. Finally, we show how the method can be extended to the study of fluid inclusion populations in order to reveal aspects of the history of the fluids before or after entrapment. Case studies on oil-bearing inclusions from Tunisia and the Alwyn oil field (North Sea) are used to illustrate this innovative aspect.

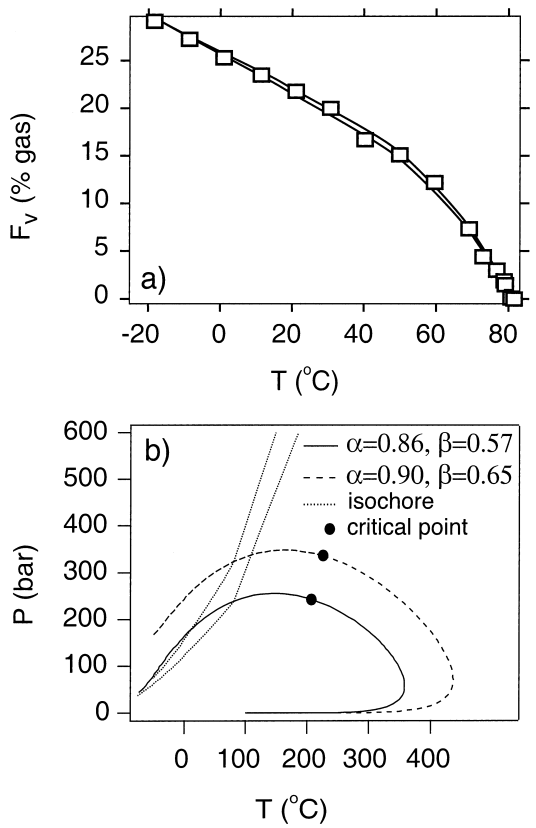

Fig. 1. (a) The variation of the degree of gas bubble filling (F_v) as a function of temperature for an oil fluid inclusion from the Alwyn field homogenising at 81.6 °C. Squares are data measured by confocal laser scanning microscopy. The superimposed curves are calculated with ($\alpha = 0.86$, $\beta = 0.57$) and ($\alpha = 0.90$, $\beta = 0.651$), respectively. (b) P–T phase diagram, calculated for the two latter (α–β) sets.

2. Thermodynamic modelling

Oils are complex mixtures, which typically contain thousands of components (paraffins, naphthenes, aromatics, etc.). Component distributions are difficult to characterize completely by conventional chemical analysis techniques. Moreover, oil thermodynamics have not advanced enough to model the behaviour of oils from raw compositional data only (Nichita, Minescu, & Cretu, 2001). Thus, we must adopt a pragmatic approach using a small number of well-defined and representative compositional and physico-chemical parameters, which can adequately model the physico-chemical behaviour of natural oils.

The key problem is the reconstruction of the phase envelope and the isochore of the trapped oil from T_h and F_v data. The oil industry is faced somewhat with a similar type of problem before the exploitation of an oil field. For safe and efficient production, the thermodynamic properties of the petroleum in the reservoir must be determined. In particular, the estimation of P–T conditions, at which the oil unmixes into gas and liquid (i.e. its bubble point curve) is crucial.

The model developed by Montel (1993), and which has been tested and validated over years on a large database of natural oil PVT properties, has been designed to estimate the gas–oil immiscibility P–T field of a reservoir petroleum. The Montel (1993) method involves taking a small quantity of the reservoir oil in a container, in order to measure two characteristic physico-chemical properties of the petroleum

at atmospheric pressure: (1) the gas/oil volume ratio (GOR), and (2) the liquid density. These properties are used as input data to the Montel method for estimating the bubble point curve of the in situ oil. We have adapted the Montel method and implemented it in our work for analysing microthermometric (T_h) and volumetric data (F_v) of oil fluid inclusions and reconstructing their phase diagrams.

To summarise the approach used in the Montel model (Montel, 1993), first, compositional analyses of reservoir oils are simplified into mixtures of 12 simple hydrocarbons (C_1, C_2, C_3, iC_4, nC_4, iC_5, nC_5, nC_6, nC_7, nC_8, nC_9, nC_{10}) and two heavier components, noted here C_{n1} and C_{n2}. These two last components, represent, in fact, two cuts of heavy molecules, respectively, C_{11-25} and C_{26+}. Obviously, this representation is a considerable simplification of the complex reality, but the model spans the whole range of molecular weights of oil components, from the lighter to the heavier ones (and is typical of oil industry practice). Then, the values of the 14 mole fractions of the hydrocarbon mixture must be defined. Fortunately, as is well known, the distribution of oil components is not arbitrary. As shown by Kissin (1987), the mole fractions of normal paraffins of high molecular weight (carbon number above 6–8) follow a geometrical law. Such a feature is taken into account in the present model: mole fractions of molecules of more than six carbon atoms obey a geometric law of exponent α. However, this law does not apply to light components (methane to hexane), as these molecules are generally in much higher quantities than those given by an extrapolation of the geometric law. This enrichment in light components is highly variable in natural oils (it is weak for heavy oils and stronger for light oils), and must be described by a second parameter, denoted β. The β parameter takes values between zero and one. The limiting case ($\beta = 0$) corresponds to a fluid, whose mole fractions are entirely described by the geometric law of α ratio. The other limiting case ($\beta = 1$) corresponds to a pure methane fluid. Other empirical corrections are included in the model, notably to take into account the relative abundance of compounds with 6–8 atoms of carbon (i.e. molecules which can be produced by the degradation of naphthenic or aromatic cycles of organic matter). However, no additional parameter is needed for this correction. The equations of the Montel (1993) compositional model are given in Appendix A.

To summarise, Montel (1993) has shown that a wide variety of natural petroleums can be adequately described by a two-parameter model. The first parameter, α, sets the amount and distribution of heavy components (C_{6+}), whereas the second one, β, is related to the methane content of the fluid. Petroleums, which are complex fluids, are replaced by simpler theoretical fluids, which are tractable to modelling and are believed to simulate closely the PVT properties of many petroleums. Such a model is known as 'compositional model' (i.e. a model that gives the mole fractions of a theoretical mixture used as a proxy of real complex natural fluids).

Once the theoretical composition of natural oil has been defined by the Montel procedure (Montel, 1993), the next step is the reconstruction of the phase diagram of natural petroleums. For this, the classical Peng–Robinson equation of state (Peng & Robinson, 1976) is used for calculating all physico-chemical properties (density, fugacities, etc.) and deriving the phase diagram.

3. Estimations of the trapping pressure and the fluid compositions

3.1. The problem

To reconstruct the phase diagram of a petroleum, we must estimate its compositional (α, β) parameters. For a reservoir petroleum, we can directly measure α and β, but how can we estimate these (α, β) parameters for petroleum trapped in a fluid inclusion? As pointed out in Section 1, compositional data are not generally available, and the only usable data are: (1) the homogenisation temperature, T_h, and (2) the degree of the gas bubble filling, F_v, measured at different temperatures.

The T_h, and F_v data are not sufficient for determining unambiguously the (α, β) parameters. In other words, the problem is underconstrained as there are two composition parameters (α and β) to estimate, and we can only use one constraint relation (that is the conservation of the bulk density of the fluid inclusion between the homogenisation point and the point, at which is measured a degree of the gas bubble filling). Thus, the problem has no unique solution: a wide range of (α, β) values can satisfy a given set of (T_h, F_v) data. An illustration is given in Fig. 1(a), where the F_v parameter of an oil inclusion from the Alwyn field (North Sea) is plotted as a function of the temperature. The inclusion homogenises at 81.6 °C. In the same plot are displayed the curves which represent the evolution of $F_v(T)$ for two different (α, β) parameters, the first one at ($\alpha = 0.86$, $\beta = 0.57$) and the second one at ($\alpha = 0.90$, $\beta = 0.651$). The former is poorer in methane and heavier components (C_{10+}) than the latter. Fig. 1(a) shows clearly that the two calculated $F_v(T)$ curves are practically superimposed and agree well with inclusion data. On the other hand, it must be noted that the phase diagrams derived from these two (α, β) parameter sets are quite different (Fig. 1(b)). Indeed, for the first one, the homogenisation pressure is 239 bar, whereas for the second one, it is equal to 324 bar. The pressure difference is more than 80 bar, and the same uncertainty will remain on the estimation of the trapping pressure. So we must admit that even precise values of degrees of gas bubble filling, as measured by confocal laser scanning microscopy, are not sufficient to constrain the modelling.

3.2. Our method

Although the problem is underconstrained, the set of (α, β) solutions is only unidimensional. Thus, we propose here to use ($\alpha-\beta$) diagrams to plot the $\beta(\alpha)$ curve, which represents graphically the whole set of solutions. As we will see below, $\beta(\alpha)$ curves can give us some important information on the nature of the petroleum, and we know that there is, at least, one (α, β) point on this curve, which is able to describe at best the PVT properties of the trapped petroleum. We will describe methods to delimit with some confidence the range of probable (α, β) values.

Taking our previous example (fluid inclusion of the Alwyn field, $T_h = 81.6\,°C$ and $F_v(0\,°C) = 25.3\%$) to illustrate our method: firstly, we calculate the $\beta(\alpha)$ curve from T_h and F_v data and plot it in a $\beta-\alpha$ diagram (Fig. 2(a)). The $\beta(\alpha)$ curve is a monotonous curve with increasing α and β values, because the α and β parameters have antagonistic effects on the size of the gas bubble. The higher is the α parameter, the richer is the fluid inclusion in heavy components, and the smaller will the gas bubble at some fixed temperature. By contrast, the higher is the β value, the richer is the inclusion in methane, and the larger will be the gas bubble. So the $\beta(\alpha)$ curve goes from low β values, representing heavy oils, to high β values, representing light volatile oils. To differentiate between these extreme petroleums, in the remainder of this section, we will develop arguments that can help us to restrict the range of possible (α, β) values on the $\beta(\alpha)$ curve.

3.2.1. GOR and API degree

First, we can have some idea about the nature of the trapped petroleum, like its GOR and its API degree. These parameters are commonly measured by petroleum geologists to characterize reservoir petroleum. Fig. 3(b) displays an $\alpha-\beta$ plot contoured with iso-GOR and iso-API degrees curves. The most characteristic values of GOR (500 and 1000 m^3/m^3) delimit the main categories of petroleum. If the GOR is below 500 m^3/m^3, the fluid is an oil; if the GOR is above 1000 m^3/m^3, this is a gas. In the field between

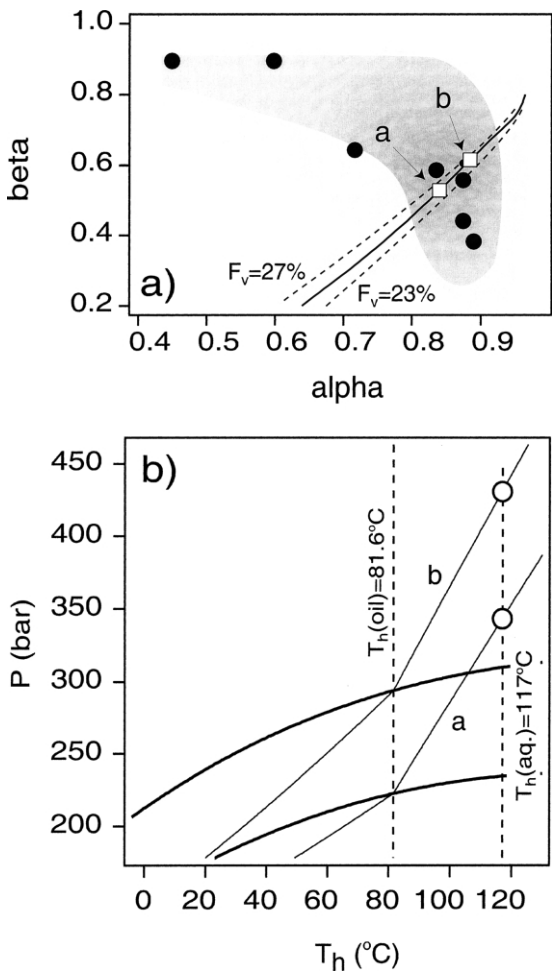

Fig. 2. (a) $\alpha-\beta$ diagram showing the ($\alpha-\beta$) curve calculated for an inclusion from the Alwyn field. Two end-member ($\alpha-\beta$) values (squares), respectively, called (a) and (b), have been chosen for this inclusion in the main correlation field (shaded area). (b) $P-T$ phase diagram, calculated for the two ($\alpha-\beta$) sets (a) and (b).

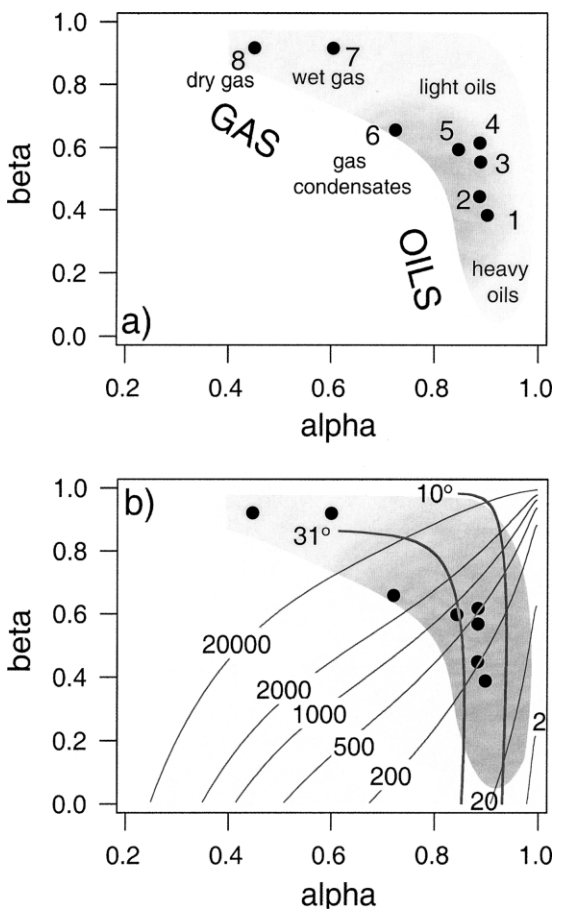

Fig. 3. The general $\alpha-\beta$ correlation existing for a wide range of natural petroleums. The shaded area delimits the region of probable ($\alpha-\beta$) values found in nature. (a) Also given are type fluids (filled circles) from the VTFlinc database: (1) heavy oil; (2) CO_2-rich oil; (3) light oil; (4) light oil; (5) 'critical' oil; (6) gas condensate; (7) wet gas; (8) dry gas. (b) Iso-GOR lines (respectively, 20 000, 2000, 1000, 500, 200, 20, and 2 m^3/m^3) and iso-API degree curves (31 and 10°).

iso-GOR curves (500 m^3/m^3) and (1000 m^3/m^3), the (α, β) point could represent an oil, a critical fluid, or a gas condensate. It can be noted that the iso-GOR lines in $\alpha-\beta$ plot follow practically the same trends than calculated $\beta(\alpha)$ curves. Iso-API curves depict an inverted L-shape in the $\alpha-\beta$ plot. These parameters are especially useful if we have some data on the reservoir petroleums of the oil field and if we suspect some similarities between the present reservoir petroleum and the studied petroleum inclusions. Thus, intersection of an iso-contour with a $\beta(\alpha)$ curve permits to obtain an estimation of the (α, β) values of a petroleum. Moreover, this allows to compare the reservoir petroleum with the inclusion oils.

3.2.2. Fluid correlation

Another way to estimate the most probable (α, β) solutions is to use a database of (α, β) values of the most common types of petroleum. Such a database can be constructed from data on fluid compositions and PVT properties of reservoir petroleum. Unfortunately, only a few data on live oils are available in the literature because of commercial confidentiality. In this study, we have integrated the small VTFlinc fluid database (Aplin et al., 1999) and other, confidential, data to calculate a database of (α, β) points. For each fluid, we have determined the (α, β) values, that most accurately reproduce the saturation pressures. Resulting (α, β) points are plotted in an (α, β) diagram (Figs. 2(a), and 3(a),(b)). The shaded area in Figs. 2(a) and 3(a) represents the most common (α, β) values of petroleums. Two main parts can be distinguished (Fig. 3): the first one corresponds to gaseous fluids, ranging from dry gas to gas condensates. Dry and wet gases, both, have β values which are close to 0.9. Values of α range from 0.4 for dry gases to 0.6 for wet gases. Gas condensates have (α, β) values around ($\alpha = 0.70-0.82$, $\beta = 0.5-0.9$). The second part corresponds to liquid petroleum, from light to heavy black oils. α values lie between 0.85 and 0.96. β values are more variable, between 0.35 for heavy oils and 0.7 for light ones. Finally, high-α ($\alpha > 0.97$) and low-β ($\beta < 0.3$) values correspond to petroleums which have been alterated. They are poor in volatiles and are enriched in heavy components. Thus, the area in the bottom-right corner of the ($\alpha-\beta$) plot is related to degassed and biodegraded petroleums. The main correlation field (shaded area of Fig. 3(a) and (b)) can help the user to restrict the range of (α, β) solutions for each calculated $\beta(\alpha)$ curve of a fluid inclusion. If we consider our Alwyn inclusion ($T_h = 81.6$ °C, $F_v = 25.3\%$ at 0 °C), we can choose a range of ($\alpha-\beta$) estimates in the main correlation field (Fig. 2(a)) and at the proximity of some points of the VTFlinc database, let us say between ($\alpha = 0.86$, $\beta = 0.57$) and ($\alpha = 0.90$, $\beta = 0.651$). This yields a pressure at the homogenisation point of 240 bar for the first estimate, and 320 bar for the second one (Fig. 2(b)). Trapping pressures are usually estimated by considering the pressure value along the isochoric path of the inclusion at the trapping temperature, supposed to be given by the homogenisation temperature of coeval aqueous inclusions (Burruss, 1992; Goldstein & Reynolds, 1994; Roedder, 1984). In our example, the homogenisation temperature of these aqueous inclusions is 117 °C. This gives trapping pressures (Fig. 2(b)) between 364 bar (for $\alpha = 0.86$, case a) and 469 bar (for $\alpha = 0.90$, case b). The range is quite large, but the lower limit (364 bar) agrees with present estimations of the past $P-T$ regime of the Alwyn field. This example shows that it is not possible to determine trapping pressures with an uncertainty lower than more or less 50 bars. Undoubtedly, this is not a very precise method of geothermobarometry, but the precision is sufficient to discriminate between hydrostatic and lithostatic pressure regimes. Fig. 2(a) shows also that uncertainties on the measured F_v degree of gas bubble filling can be neglected. Dashed $\beta(\alpha)$ curves have been calculated, respectively, for a filling degree F_v of 23 and 27%, i.e. simulating the consequences of a relative error of 10% on the filling degree. Note that the three $\beta(\alpha)$ curves are practically coincident in the shaded area of the (α, β) plot.

3.2.3. IR spectroscopy

Other characterization methods for petroleum inclusions can help us to improve the (α, β) estimation. For example, IR spectroscopy can give some indications about the composition. In particular, the ratio of the peak areas of to the $-CH_2$ and $-CH_3$ functional groups gives us some information about the bulk composition of fluid inclusions (Pironon & Barrès, 1990, 1992). The higher the ratio will be, the more the fluid will contain long-chain molecules, and the lower will be the β value. FT-IR spectroscopy (Pironon, Thiéry, Teinturier, & Walgenwitz, 2000) gives also information about the gas content of fluid inclusions. Methane/alkane concentration ratio is estimated after decomposition of the CH-stretching area, and the CO_2/CH_4 concentration ratio is calculated from CO_2 stretching area.

3.3. Influence of water

Another problem, which must be addressed for the calculation of isochores, is linked to the presence of water in fluid inclusions. Indeed, oil-bearing fluid inclusions can contain a large amount of water. The invisible aqueous film, which is wetting the walls, can represent an amount as high as 25% mole fraction of the bulk composition of the fluid inclusion. The difference between the thermal expansitivity of the aqueous phase and the petroleum become significant above 100 °C and can influence the evolution of the internal pressure. For example, Bodnar (1999) has shown that water in CO_2 fluid inclusions, although invisible, can affect a lot the estimations of trapping pressures. This effect is never taken into account in petroleum inclusions, as they are assumed to be filled only with hydrocarbons.

Therefore, we have used the Daridon equation of state (1992), which is one of the few thermodynamic models that

can represent gas–liquid phase transitions in water–paraffins systems, to investigate whether the presence of water in inclusions containing both oil and water would affect the PVT properties of the oil and thus invalidate use of the simpler Peng–Robinson formulation. Calculations show that water has only a minor influence on the isochoric paths in the range of the trapping temperatures usually found in oil fields (100–150 °C). Effective trapping pressures are underestimated by a few bars: so there is no need to use a more sophisticated equation of state like the Daridon equation of state (Daridon, 1992; Daridon, Lagourette, Saint-Guirons, & Xans, 1993), and the Peng–Robinson equation of state (Peng & Robinson, 1976) remains valid for calculating isochores.

3.4. Analogies and differences of our method with the VTFlinc software

Our method and the VTFlinc software (Aplin et al., 1999) can both be used to analyse (T_h, F_v) data of petroleum fluid inclusions. They produce similar $P-T$ phase diagrams, as they are based on the same thermodynamic models using cubic equations of state like the Peng–Robinson equation of state (Peng & Robinson, 1976). In some cases, both methods fail to reproduce observed F_v curve, whose shape differs from the usual convex curve as seen in Fig. 1(a), and exhibits an additional inflexion point. This situation may be linked to solid phases precipitation below the homogenisation point.

On the other hand, our approach is clearly different from the VTFlinc software (Aplin et al., 1999). In the method used by VTFlinc, the user selects a priori an initial composition between several types of petroleum (black oil, light oil, gas condensate, etc.) in a fluid database. Then the program finds an optimum composition by fitting the calculated degrees of gas bubble filling against F_v data with an iterative minimization algorithm. At each iterative step, VTFlinc adds or removes a small amount of 'titrant' gas, whose composition is also calculated by VTFlinc. Several options are proposed to the user for calculating the composition of the titrant gas (Aplin et al., 1999). As the problem has many degrees of freedom, there are as many solutions as initial compositions. Thus, several oil compositions must be calculated in order to taste how they influence the final results. The innovative part of our approach is the use of a compositional model (Montel, 1993). It allows to transform a complex multidimensional problem to an unidimensional one, which is more tractable. The whole set of solutions can be visualized by a $\beta(\alpha)$ curve. Thus, on a single plot, one can evaluate at once how a composition change can modify the nature of the petroleum, its GOR and its API degree. However, both methods produce similar uncertainty on pressure estimates, but the slight advantage of our method is that it is made more explicit.

Another interesting point of the (α, β) method is the possibility to compare between the trapped oils and reservoir oils. It is indeed possible to estimate the (α, β) parameters of the reservoir oil from its GOR and its saturation pressure. The corresponding reservoir (α, β) point can be plotted in the ($\alpha-\beta$) plot in order to follow the evolution from past inclusion oils to the present reservoir petroleum. The method presented in this part can also be used in the other way: if the past entrapment pressure and temperature are also known, it is possible to set precisely the (α, β) parameters of the trapped fluid along its $\beta(\alpha)$ curve. Such information is extremely valuable, as this allows to get useful indications on the processes that have affected oils either before or after entrapment (Section 4).

4. Process simulations

During its migration, oil can be altered by various processes: liquid–gas unmixing, petroleum mixing, leaching by a gas or an aqueous solution, biodegradation, gravity segregation, etc. All of these phenomena can be recorded in petroleum fluid inclusions, as they trap successive aliquots of migrating or evolving fluids. After entrapment, other processes (Goldstein & Reynolds, 1994; Roedder, 1984) can also alter the properties of inclusions (e.g. leakage, necking down, chemical reactions, decrepitation, implosion). Thus, it is not rare to observe very different (F_v-T_h) characteristics in a population of oil fluid inclusions in the same sample. The present method offers us the opportunity to analyse the causes of these (F_v-T_h) differences. In this part, we have simulated the effects of some of these processes on the microthermometric (F_v-T_h) properties of successive fluid inclusions. Not every process has not been studied in this work. This includes in particular: water washing (McAuliffe, 1979), biodegradation, oil cracking, etc. However, this study will give use some clues for analysing further natural petroleum inclusions.

4.1. Fluid pressure and/or temperature variations

Fluid pressure and/or temperature variations commonly occur during the evolution of reservoirs. Pressure variations may occur, for example, when fractures are opened because of the overpressure exerted by fluids, at the lithostatic limit, resulting in a strong decrease of the fluid pressure. Burial of a reservoir or its uplift lead also to simultaneous pressure–temperature changes. In the case where the pressure decrease is not sufficient to cause a liquid–gas unmixing (Section 4.2), any fluid inclusions subsequently trapped will have the same bulk composition as those trapped beforehand. The qualitative effects of an isothermal decompression are shown in Fig. 4 for a petroleum of ($\alpha = 0.895$, $\beta = 0.39$) parameters. In a first case, we have considered a pressure decrease from 251 bar (point a) to 175 bar (point b) at 110 °C. We observe that the homogenisation temperature increases from 81.7 to 100 °C. Concomitantly, the degree of gas bubble filling at 0 °C increases from 10.2 to 12.7%. Such

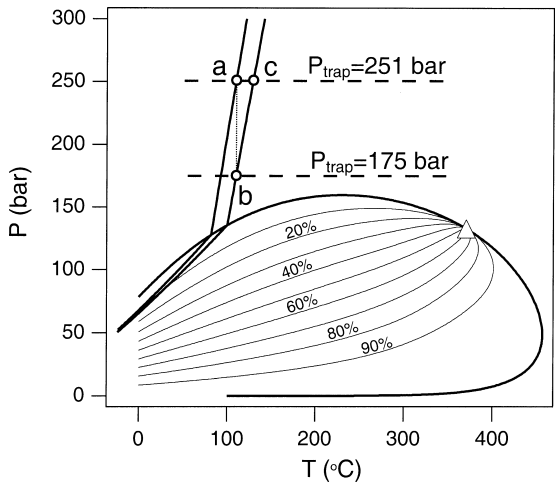

Fig. 4. P–T diagram illustrating the effects of a decrease of the trapping pressure (from a to b) or an increase of the trapping temperature (from a to c) on the (T_h–F_v) properties of oil fluid inclusions. Coordinates of the trapping points are: (a) $P_{trap} = 251$ bar, $T_{trap} = 110$ °C, (b) $P_{trap} = 175$ bar, $T_{trap} = 110$ °C, (c) $P_{trap} = 251$ bar, $T_{trap} = 120$ °C. The phase envelope and isochores are calculated for an oil of $\alpha = 0.895$ and $\beta = 0.39$. Thin solid curves labelled in percentages are iso-F_v curves.

variations of (F_v–T_h) properties can also be generated by an isobaric heating of the reservoir (Fig. 4). In our example, heating of the reservoir from 110 °C (point a) to 120 °C (point c) at 251 bar produces exactly the same result.

Thus, our method cannot discernate the relative contribution of pressure and temperature changes. As this process does not modify the composition of the successive fluid inclusions, $\beta(\alpha)$ curves must coincide on the (α–β) plot. This process can be identified if there is a positive correlation between T_h and F_v data and a good superposition of $\beta(\alpha)$ curves on the (β–α) plot (but be careful, other processes can also produce the same results, see below). More detailed results of numerical simulation are displayed in Fig. 5(b). We have considered here the case of a fluid of ($\alpha = 0.895$, $\beta = 0.39$) parameters. This is a heavy black oil, represented by point 1 in Fig. 5(a). Successive T_h and F_v (at 20 °C) have been calculated by letting the fluid pressure decrease from 300 to 200 bar at a fixed temperature of 100 °C. Decompression leads to an increase of both T_h and F_v (Fig. 5(b)). The lowest T_h and F_v values represent oils that have the highest densities. Such a trend can also be produced by a temperature variation.

4.2. Gas inputs in a sealed reservoir

Reservoir oils can receive successive charges of gas migrating from deeper zones or biogenic gas from other levels. Such a process will cause enrichment of oil in methane. We consider here the model of a sealed reservoir, where no fluid can escape. The reservoir is initially filled with a heavy black oil of parameters ($\alpha = 0.94$ and $\beta = 0.2$). Reservoir pressure and temperature are set at 300 and 100 °C. It is assumed that gas inputs will not increase

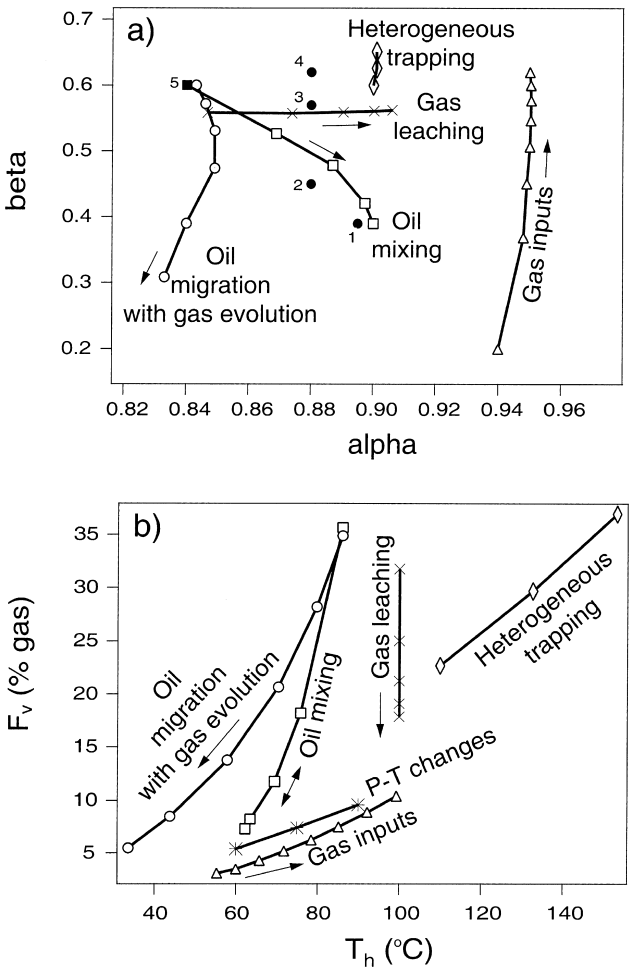

Fig. 5. Effects of different processes on the characteristics of oil fluid inclusions in (a) an (α–β) diagram and (b) a (T_h–F_v) plot. Small filled circles represent (α–β) points of the correlation established from the VTFlinc database. Following processes are depicted: oil migration with gas phase separation (empty circles), oil mixing (empty squares), gas leaching (crosses), gas inputs (triangles), heterogeneous trapping (diamonds), and pressure–temperature variations (stars).

significantly the pressure. At each addition of gas (0.1 mol of methane per mole of oil), the new (α–β) characteristics of the resulting fluid have been calculated from its (T_h–F_v) values. The evolution of (α–β) parameters are given in Fig. 5(a). A strong increase of the β value is observed. On the contrary, α remains almost constant. In Fig. 5(b), the (F_v–T_h) curve exhibits a trend, that looks similar to pressure–temperature variations, as described above.

4.3. Mixing of two oils

The mixing of two homogeneous oils is a process which is probably common in oil reservoirs, e.g. as successive charges mix. We consider the case of mixing of a light crude, oil A, ($\alpha = 0.84$, $\beta = 0.6$), and a heavier crude, oil B, ($\alpha = 0.90$, $\beta = 0.39$). The mixing temperature and pressure have been set at 100 °C and 300 bar. We have calculated the characteristics of oil fluid inclusions trapping various

proportions of (A) and (B) oils. The resulting $\beta(\alpha)$ curve is given in Fig. 5(a), and the (T_h, F_v) values are plotted in Fig. 5(b). Heavy (B) oil has T_h and F_v values ($T_h = 62.2$ °C, $F_v = 7\%$ at 0 °C) lower than the light one ($T_h = 86$ °C, $F_v = 36\%$ at 0 °C). Note that T_h and F_v values of light (A) oil decrease quickly as slight amounts of heavy (B) oil are added. On the other hand, inputs of light oils have less pronounced effects on heavy oils.

4.4. Oil migration with gas evolution

During migration to shallower levels, petroleum undergoes decreases of pressure and temperature that may cause liquid–gas unmixing (Silverman, 1963). As the gas is less dense, it will escape from oil. This phenomenon will produce residual petroleums that become more and more depleted in light ends (methane, ethane, etc.) as the process proceeds. To describe this phenomenon, we have considered the migration of a light oil ($\alpha = 0.84$ and $\beta = 0.6$), starting at 100 °C and 300 bar, and which migrates along a geotherm of 33 °C/km to shallower levels. The oil reaches gas saturation at 86 °C and 258 bar. From this point, oil continues its migration until the gas supersaturation is so high that gas escapes. The composition of the depleted oil and its new saturation conditions $P_h^{sat}(T)$ are recalculated. Then, new (α–β) parameters are fitted in order to reproduce the bubble point curve of the oil. This procedure has been repeated several times along the geotherm. The first evolved fluids are gas condensates, which progressively evolve through wet to dry gases. α values of residual oils increase, then decrease slightly, whereas β parameters decrease strongly. Thus, the $\beta(\alpha)$ curve is almost vertical, as shown on the (α–β) diagram (Fig. 5(a)).

This process could be represented by compositional variations in successive generations of fluid inclusions (Bodnar, 1990). Its occurrence could also be suggested in a single sample by heterogeneous trapping of oil and gas (Goldstein & Reynolds, 1994), as explained below.

4.5. Heterogeneous trapping of oil and gas

Up to now, we have been considering the trapping of an homogeneous fluid. It may happen that an oil phase coexists with a gas in the pore space. Such a phenomenon will lead to the trapping of various amounts of gas and oils in fluid inclusions, a process generally known as *heterogeneous trapping* (Roedder, 1984). Such a process has been simulated by considering a light oil of ($\alpha = 0.9$ and $\beta = 0.6$) parameters, at 90 °C and 248 bar. At these P–T conditions, the petroleum unmixes into a mixture of gas (5 vol%) and oil (95 vol%). The residual oil has compositional properties which are close to the initial petroleum ($\alpha = 0.9$ and $\beta = 0.58$), whereas the gas is a gas condensate ($\alpha = 0.77$ and $\beta = 0.8$). We have calculated (T_h–F_v) and (α–β) properties of inclusions trapping mixtures of (0–100%), (10–90%) and (20–80%) volume percent of gas and oil, i.e. high-density inclusions homogenising to liquid.

Calculations show that α is unchanged, whereas β increases with the gas amount trapped in these inclusions (Fig. 5(a)). The inclusions, which trap the residual oil, will exhibit the lowest T_h and F_v values. Inclusions trapping a mechanical mixture of oil and gas, are characterized by higher T_h and F_v parameters. The higher the T_h, the higher is F_v measured at a given temperature would be. Thus, heterogeneous trapping can be recognized by a positive correlation between T_h and F_v in a (T_h–F_v) diagram (Fig. 5(b)). Other processes (P–T changes, gas inputs, etc.) produce also the same characteristics, but the variation in F_v is qualitatively greater in the case of heteregeneous trapping (Fig. 5(b)). This process can also generate gas inclusions, trapping the gas end-member pole. These inclusions have a low density and will homogenise to vapour.

4.6. Open system gas leaching

Another possible alteration process in reservoir oils is gas leaching, also named evaporative fractionation (Larter & Mills, 1990; Meulbroek, Cathles, & Whelan, 1998; Thompson, 1987; Thompson, 1988). This is the migration of a gas, predominantly composed of methane, through an open-system oil reservoir. First inputs of methane saturate the oil. Then the whole system remains heterogeneous as an emulsion of gas in oil. The most volatile compounds in oil (ethane, propane, etc.) are then extracted by the methane gas. As the system is open, these components are leached away when the gas escapes. Methane content in the oil remains roughly constant.

To illustrate this effect, we consider the case of a gas–saturated oil, characterized by ($\alpha = 0.847$ and $\beta = 0.559$) parameters at 100 °C and 240 bar. At each step of the process, a small amount of methane is added to the system producing liquid–gas immiscibility. After equilibrium with oil, the gas is removed. Then, the composition of the residual oil is calculated. Eventually, the new (α–β) characteristics of the residual oil are recalculated. The resulting $\beta(\alpha)$ curve is given in Fig. 5(a). In contrast to the previous case, this curve is almost horizontal: α increases, whereas β remains constant. On Fig. 5(b), T_h remains constant at 100 °C, but F_v drastically decreases.

4.7. Density and composition changes of inclusions after entrapment—stretching, leakage, necking-down

The last processes we consider are those produced by post-trapping phenomena: stretching, leakage, or necking down of fluid inclusions. Stretching is the simplest one, as to a first approximation, it modifies only the bulk density, but not its bulk composition. As a result, this process produces variations of the (T_h, F_v) properties, which are equivalent to those produced by pressure–temperature variations

(Section 4.1). Thus, this phenomenon can be identified by a positive correlation of (T_h, F_v) properties and practically coincident $\beta(\alpha)$ curves on an ($\alpha-\beta$) plot.

Necking down and leakage of biphasic liquid–gas inclusions are much more complex, as they modify both the bulk density and composition. The consequences are similar to those produced by heterogeneous trapping of gas and oil (Section 4.5). As a result, this produces fluid inclusions with variable (T_h, F_v) data, and $\beta(\alpha)$ curves will not coincide on the $\alpha-\beta$ plot.

5. Case studies

5.1. Oil inclusions from Jebel Guebli (Tunisia)

Petroleum inclusions from Boujabeur (Jebel Guebli, south of Tunis) are trapped in fluorite. They are spherical, two-phase, yellow coloured in transmitted light. These inclusions homogenise to liquid between 110 and 135 °C, and are associated with planes of aqueous inclusions with T_h varying between 110 and 140 °C and salinity lying between 15 and 17 wt% NaCl equivalent (Bouhlel, Fortuné, Guilhaumou, & Touray, 1988; Guilhaumou, Touray, & Bouhlel, 1988). Petroleum inclusions do not belong to the aqueous inclusions planes but are located in the proximity. Some petroleum inclusions have decrepitated, others are affected by fracturing. The histogram of homogenisation temperatures for petroleum inclusions is asymmetric towards high temperatures, suggesting post-trapping events such as leakage or stretching. Leakage of biphasic inclusions changes both the bulk density and composition, whereas stretching does not modify the composition.

To determine the nature of the post-trapping event, two oil fluid inclusions (a) and (b) in fluorite from Jebel Guebli (Tunisia) located in the same array have been considered in detail. They present clearly distinct (F_v-T_h) characteristics. The first one homogenises at 110.1 °C and has a F_v of 9.5% at 20 °C, whereas the second one homogenises at 132.6 °C and has a similar F_v of 10.9% at 20 °C. They belong to the extreme parts of the histogram of homogenisation temperatures.

Fig. 6 shows the calculated ($\alpha-\beta$) curves for these two inclusions, which are almost coincident. These curves are located in the field of black oils (GOR between 30 and 120 m^3/m^3). The good superposition of the $\beta(\alpha)$ curves suggest that both inclusions may have the same bulk composition. FT-IR spectroscopy reveals similar methane content in both inclusions, between between 10 and 20 mol%. We have chosen the following values $\alpha = 0.92$ and $\beta = 0.333$ at the intersection of the $\beta(\alpha)$ curves with the main correlation field (shaded area of Fig. 6). This yields a GOR of 62 m^3/m^3 and a methane content of 22%. This concentration is in good agreement with the methane content estimated by FT-IR. Thus, infrared data suggest that the choice of the ($\alpha-\beta$) parameters is good. It can be concluded that the post-trapping event affecting the inclusions is not marked by a change of composition and then should be attributed to a stretching process.

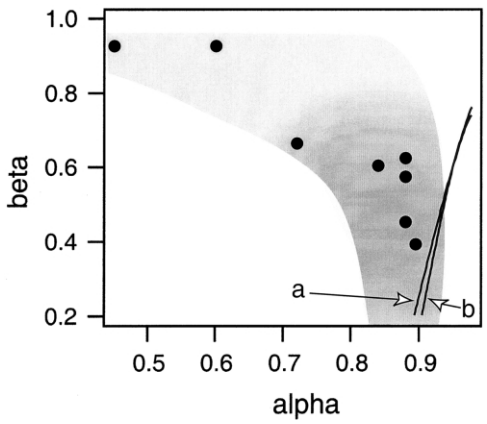

Fig. 6. $\alpha-\beta$ plot showing the $\beta(\alpha)$ curves of two oil-bearing inclusions (a) and (b) in fluorite. See text for discussion.

5.2. Oil inclusions of the Alwyn field

A series of eight petroleum inclusions of the Alwyn field (North Sea) provide a second demonstration of the method. They have been studied in two samples of sandstones from the Brent formation. Analytical data for the inclusions are presented in Table 1. Six inclusions (3a–3d, 4a and 4b) are trapped in a healed microfracture crossing a quartz grain. This sample comes from one well at 3616.33 m in depth. The larger (3a) has a complex shape and a length of 80 μm. It is surrounded by tiny satellite (3b–3d) inclusions (less than 10 μm). This feature suggests tiny inclusions being produced from necking-down of the originally large inclusion (3a). Inclusion (4a) has an intermediate size (25 μm) and is of simpler form. It is near a smaller inclusion (4b). These inclusions are associated with aqueous inclusions homogenising at 105 °C. Two other large inclusions (5 and 6) come from a second well at a depth of 3700 m and are also in a healed microfracture in a quartz grain. Associated aqueous inclusions homogenise at 117 °C and have been described in Dubessy, Buschaert, Lamb, Pironon, and Thiéry (2001).

Table 1
Characteristics (T_h, F_v) of eight fluid inclusions of the Alwyn field

Inclusion	T_h (°C)	F_v (% gas) at 20 °C
3a	94.7	25
3b	84.0	7.9
3c	84.1	6.0
3d	83.4	3.4
4a	86.1	6.3
4b	82.2	12.7
5	81.6	21.8
6	81.9	19.9

T_h–F_v characteristics of these inclusions are plotted in Fig. 7(a). Resulting $\beta(\alpha)$ curves are given in Fig. 7(b). Different degrees of superimposition of $\beta(\alpha)$ curves show significant compositional similarities and differences between these inclusions. Inclusions in the first sample clearly have different oil compositions. The $\beta(\alpha)$ curve of the large inclusion (3a) is characteristic of a volatile oil (GOR around 500 m^3/m^3), whereas inclusions (3b–3d) are black oils with a GOR between 20 and 100 m^3/m^3 (Fig. 7(b)). In the same sample, inclusion (4a) traps a black oil similar to inclusion (3b). Inclusion (4a) has compositional characteristics which are intermediate between inclusion (3a) and other inclusions (3b–3d and 4b). In the second sample, $\beta(\alpha)$ curves of inclusions (5) and (6) superimpose almost perfectly on the $\beta(\alpha)$ curve of inclusion (3a), although they do not come from the same well and do not have the same homogenisation temperatures. Thus, we can assume that the large inclusions (3a, 5 and 6) contain the same petroleum, a volatile oil having a GOR of 500 m^3/m^3.

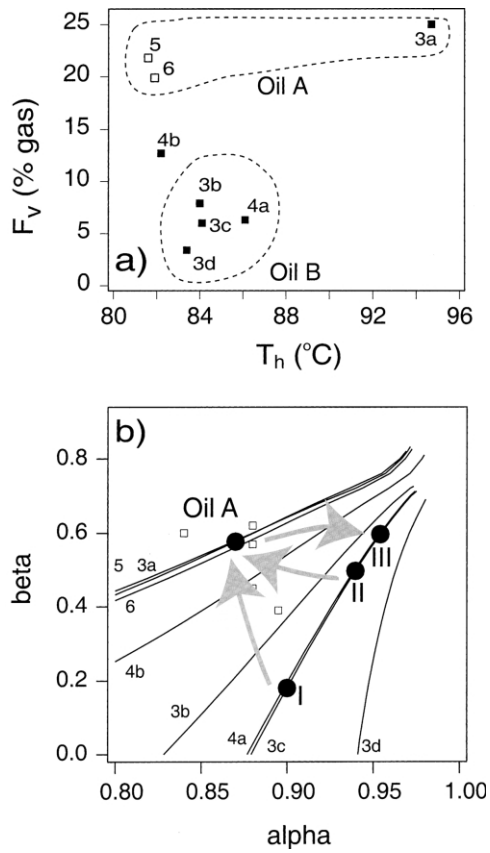

Fig. 7. Petroleum inclusions of the Alwyn field. (a) T_h–F_v characteristics in a (T_h–F_v) plot and (b) interpretation of composition evolution in an (α–β) diagram. Arabic numbers refer to fluid inclusions. In Fig. 7(a), petroleum inclusions of similar (α–β) composition are grouped together. Inclusions 3a, 3b, 3c, 3d, 4a and 4b (filled squares) come from one well, inclusions 5 and 6 (empty squares) from another one. In Fig. 7(b), the possible (α–β) parameters of oils A and B are represented by filled circles. Three cases are discussed (I–III) for the composition of oil B in the text. Small empty rectangles represent (α–β) points of the VTFlinc petroleum database (Fig. 3(a)). Arrows indicate the evolution direction.

For the remainder of the discussion, we will call this petroleum, oil A. The heavier black oils contained in smaller inclusions (3b–3d and 4a) will be referred to as oil B. Inclusion (4b) contains a petroleum, intermediate between oils A and B. In the following sections, we develop arguments which show how the two oils may be genetically related and consider a number of processes.

5.2.1. Composition of oils A and B

For the composition of oil A, we have chosen the following values $\alpha = 0.87$ and $\beta = 0.5772$. This (α–β) point belongs to the $\beta(\alpha)$ curve of inclusion (3a) and has been selected in the field of the main correlation. Thus, it is representative of common volatile oils existing in nature. The GOR is 476 m^3/m^3. Calculations indicate a methane content of 54 mol%. This latter value is confirmed by FT-IR analysis (50 mol%). Homogenisation temperatures of inclusions (5) and (6) are 81.6 and 81.9 °C, respectively, and are lower than the homogenisation temperature (94.7 °C) of inclusion (3a). This feature indicates a higher density for inclusions (5) and (6).

Estimation of the composition of oil B is more problematic, as inclusions (3b–3d and 4a) cannot be analysed by FT-IR spectroscopy because of their size. Inclusions (3c) and (4a) are thought to be the most representative of oil B. Inclusion (3d) seems to contains an heavier oil, but this must be considered with caution. Inclusion (3d) has a small size (less than 10 μm) and only a very small gas bubble. If we take into account the large uncertainty on the F_v value of this inclusion, it is possible that the inclusion (3d) has a similar composition to inclusions (3c) and (4a).

In the following, we will test and discuss three sets of (α–β) parameters for oil B, that we have selected along the $\beta(\alpha)$ curve of inclusion (3c), from low to high β values.

5.2.2. Scenario I

For the composition of oil B, we first consider the values $\alpha = 0.90$ and $\beta = 0.1805$, giving a GOR of 47 m^3/m^3. Compared with oil A, the isopleth of oil B is shifted towards low pressure and high temperature (Fig. 8(a)). The isochores of the oils A and B are roughly parallel in the (P–T) diagram and do not intersect. Isochore of oil B is around 50 bar below the isochore of oil A, indicating slightly different P–T trapping conditions. In this scenario, oils A and B have similar α values, but very different β parameters. Such a situation can be produced by gas inputs in a sealed reservoir (Section 4.2). Oil B would have been the initial petroleum in the reservoir. Successive charges of gas would have progressively enriched the sealed reservoir in volatiles, explaining the evolution of initial oil B to oil A. We have represented this trend in the (α–β) plot (Fig. 7(b)) by a line denoted I, running from the (α, β) point of oil B to the (α, β) point of oil A.

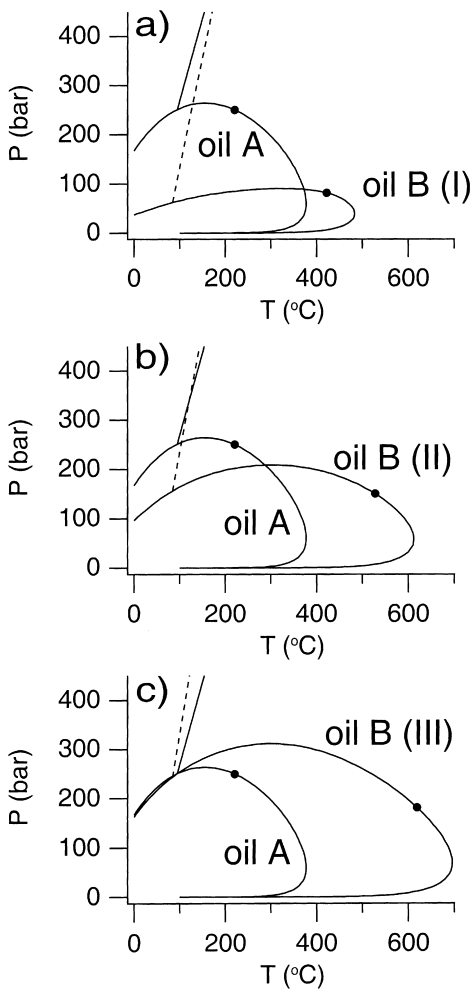

Fig. 8. $P-T$ diagrams showing the possible scenarios of the evolution of petroleum fluid inclusions of the Alwyn field. (a) Scenario I (oil B: $\alpha = 0.90$, $\beta = 0.1805$): gas inputs in a sealed reservoir. (b) Scenario II (oil B: $\alpha = 0.9397$, $\beta = 0.4969$): oil mixing of oils A and B. (c) Scenario III (oil B: $\alpha = 0.9397$, $\beta = 0.4969$): heterogeneous trapping, or necking down, or gas leaching. Note the relative position of the isochore of oil B (dotted line) against the isochore of oil A (see text for discussion).

5.2.3. Scenario II

We consider now the values $\alpha = 0.9397$ and $\beta = 0.4969$, giving a GOR of 90 m^3/m^3 for oil B. By increasing the β value, the isopleth of oil B expands to higher pressures and higher temperatures (Fig. 8(b)). Saturation pressures of oils B increase and move towards saturation pressures of oils A. Note that the isochores of oils A and B intersect now (Fig. 8(b)). Thus, oils A and B can be trapped at the same $P-T$ conditions. The calculated trapping pressure is 360 bar, which corresponds to the hydrostatic pressure at the present time. Oils A and B would be two distinct petroleums that have been trapped at different times, but at similar $P-T$ conditions. Inclusion (4b) would correspond to a mixing of oils A and B.

5.2.4. Scenario III

Finally, we consider the values $\alpha = 0.954$ and $\beta = 0.5966$, giving a GOR of 100 m^3/m^3 for oil B. In this case (Fig. 8(c)), saturation pressures of oil B are similar to the saturation pressures of oil A, and the isochore of oil B is shifted towards lower temperatures and higher pressures with respect to the isochore of oil A. The similarity of saturation pressures of oils A and B allows to suggest several processes, either (1) inclusions (3a–3d) have been produced by necking down of biphasic petroleum inclusions, or (2) inclusions (3a–3d) have been produced by heterogeneous trapping of a gas–oil mixture, or (3) oil B derives from oil A by gas leaching.

Petrographic observations are partly in favour of necking down (hypothesis 1). Initially, petroleum was trapped in large inclusions. Subsequent evolution leads to unmixing of gas and oil in the inclusions and to necking down of these initial large biphasic inclusions (e.g. 3a). Tiny satellite inclusions (e.g. 3b, 3c and 3d) formed from the edges on the inclusion, trapping residual oil B, enriched in heavy components. Thus, inclusion 3a, trapping a mechanical mixture of gas condensate and oil B, has a lower density, thus explaining the higher homogenisation temperature ($T_h = 94.7$ °C) of inclusion (3a) compared to other inclusions (3b–3d, $T_h = 82–84$ °C). Hypothesis 2 (heterogeneous trapping of a gas–oil mixture) is essentially the same as the first one. It implies that gas–oil unmixing of the initial petroleum occurred before the trapping of fluids.

Hypothesis 3 (gas leaching) can also be suggested. As discussed in Section 4.6, gas leaching produces oils with increasing α and constant β parameters (Fig. 7(b), line denoted III). The initial fluid would have been represented by a light oil (A) and would have been subsequently leached by methane gas. This would have depleted (A) fluids in their components of medium molecular weight (from ethane to octane), and produce (B) oils, both enriched in methane and heavier components (C_{8+}). However, gas leaching does not explain the lower T_h of inclusions (3b–3d). The difference (around 10 °C) is relatively small, and can be produced by an increasing of the pressure (an increase of 100 bar is sufficient to decrease the homogenisation temperature by 10 °C).

6. Conclusion

A new method is proposed for the analysis and interpretation of microthermometric and volumetric measurements performed on oil fluid inclusions. Its main innovation stems from the use of a compositional model (Montel, 1993) applicable to the broad spectrum of natural petroleums. This model uses two parameters only, called α and β, that describe the distribution of components. Therefore, it provides a simple way of characterizing the composition of an oil. Combined with equations of state (Peng & Robinson, 1976), this model allows numerous physico-chemical properties of interest to be estimated, such as: $P-T$ immiscibility loops, or isochoric paths of trapped oils. Applications of the method are given for oil-bearing inclusions from Tunisia and the Alwyn field. We show how

the method can give constraints on the trapping pressures of fluids, although we conclude that paleobarometry based on fluid inclusion measurements can have large errors (around 50–100 bar). Perhaps more significantly, insights can also be obtained on the various processes affecting fluids before or after entrapment. Plotting and comparison of $\beta(\alpha)$ curves of fluid inclusions can reveal whether one or more distinct fluids have been trapped. Working hypotheses about the various alteration processes (gas leaching, gas inputs, oil mixing, etc.) can be evaluated. However, different processes can have similar effects, and complementary data from independent methods are required to discriminate these. Software, including the equations of the compositional model of Montel (1993) and the calculation algorithms of $\beta(\alpha)$ curves and phase diagrams will be the subject of another publication.

Acknowledgements

We are grateful to Dr Norman Oxtoby for his careful review, that helped us to improve an earlier version of this manuscript. We thank also Prof. D. G. Roberts for his constructive comments.

Appendix A

A.1. The compositional model of Montel (1993)

These equations are part of the compositional model of Montel (1993), that define the component distribution of a petroleum.

To simplify the notations, let's call q_n, the number of moles of the hydrocarbon component having n atoms of carbon (n ranging from 1 to 500).

We start with:

$$q_1 = 1, \tag{A1}$$

$$q_2 = \alpha(1-\beta), \tag{A2}$$

then, from $n = 2$ to 5

$$q_{n+1} = q_n\alpha(1-\beta/n^{0.5}) \tag{A3}$$

and

$$q_7 = q_6, \tag{A4}$$

and then, for n above 7

$$q_{n+1} = q_n\alpha(1-\beta/n). \tag{A5}$$

The two heavier cuts $q(C_{n1})$ and $q(C_{n2})$ are calculated by:

$$q(C_{n1}) = q_{11} + q_{12} + \cdots + q_{25}, \tag{A6}$$

$$q(C_{n2}) = q_{26} + q_{27} + \cdots \tag{A7}$$

The mole numbers of ethane to pentane (q'_2, q'_3, q'_4 and q'_5) are corrected as follows:

$$s = 0.94(q_3+q_4+q_5)(q_1(1.8-q_1))^{0.5}, \tag{A8}$$

$$q'_2 = 0.976725s(0.19+q_1), \tag{A9}$$

$$q'_3 = 0.4341s, \tag{A10}$$

$$q'_4 = q_3\alpha/(0.8+\beta), \tag{A11}$$

$$q'_5 = q_4\alpha/(0.9+0.7\,\beta^2). \tag{A12}$$

The mole numbers of iC_4, nC_4, iC_5 and nC_5 are given by:

$$q'_{iC4} = q'_4/3.24, \tag{A13}$$

$$q'_{nC4} = q'_4/1.4465, \tag{A14}$$

$$q'_{iC5} = q'_5/1.86207, \tag{A15}$$

$$q'_{nC5} = q'_5/1.16,. \tag{A16}$$

The corrected mole numbers from hexane to decane are calculated by:

$$q'_n = q_n(0.3936+0.0574n)(1+10(\alpha-0.9)^2). \tag{A17}$$

Finally, the mole fraction z_i of component i (i = C_1, C_2, C_3, iC_4, nC_4, iC_5, nC_5, nC_6, nC_7, nC_8, nC_9, nC_{10}, C_{n1}, C_{n2}) in the mixture is given by:

$$z_i = q'_i/(q_1+q'_2+q'_3+q'_{iC4}+q'_{nC4}+q'_{iC5} + q'_{nC5},+q'_6+q'_7+q'_8+q'_9+q'_{C_{n1}}+q'_{C_{n2}}). \tag{A18}$$

References

Aplin, A. C., Mcleod, G., Larter, S. R., Pedersen, K. S., Sorensen, H., & Booth, T. (1999). Combined use of confocal laser microscopy and PVT simulation for estimating the composition and physical properties of petroleum in fluid inclusions. *Marine and Petroleum Geology*, *16*, 97–110.

Bodnar, R. J. (1990). Petroleum migration in the Miocene Monterey Formation, California, USA: Constraints from fluid inclusion studies. *Mineralogical Magazine*, *54*, 295–304.

Bodnar, R. J. (1999). The effect of small (undetectable) amounts of water on pressure determinations from carbon dioxide inclusions (Abstract). ECROFI XV, *European Conference on Research on Fluid Inclusions XV*, 21–24 juin, Potsdam, Germany.

Bouhlel, S., Fortune, J. P., Guilhaumou, N., & Touray, J. C. (1988). Les minéralisations stratiformes à F–Ba de Hammam Zriba, Djebel Guebli (Tunisie Nord-orientale): Cadre géologique et conditions de genèse, apport de l'étude des inclusions fluides. *Mineralia Deposita*, *23*, 166–173.

Bratus, M. D., Svoren, I. M., & Danysh, V. V. (1975). Inclusions of hydrocarbons in 'Marmorosh diamonds' from Carpathians as indicators of migration of oil fluids. Carbon and its compounds in endogenic processes of mineral formation (Abstract). *COFFI, Conference on Fluid Inclusions, Vol. 8* (p. 28).

Burruss, R. C. (1987). Crushing-cell, capillary column gas chromatography of petroleum fluid inclusions: Method and application to petroleum source rocks, reservoirs and low temperature hydrothermal

ores (Abstract). *PACROFI III, Pan American Conference On Research on Fluid Inclusions. Program and Abstracts*, Socorro, NM, (unpaginated).

Burruss, R. C. (1992). Phase behaviour in petroleum–water (brine) systems applied to fluid inclusion studies (Abstract). *PACROFI IV, Pan American Conference on Research on Fluid Inclusions, Program and Abstracts, Vol. 4* (pp. 116–118), Lake Arrowhead, CA.

Daridon, J. -L. (1992). *Mesure et représentation des équilibres de phases sous pression de mélanges d'eau, de paraffines et de dioxyde de carbone* (p. 177). PhD, Université de Pau et des Pays de l'Adour.

Daridon, J. L., Lagourette, B., Saint-Guirons, H., & Xans, P. (1993). A cubic equation of state model for phase equilibrium calculation of alkane + carbon dioxide + water using a group contribution k_{ij}. *Fluid Phase Equilibria*, *91*, 31–54.

Dubessy, J., Buschaert, S., Lamb, L., Pironon, J., & Thiéry, R. (2001). Methane-bearing aqueous fluid inclusions: Raman analysis, thermodynamic modelling and application to petroleum basins. *Chemical Geology*, *173*, 193–205.

George, S. C., Ruble, T. E., Dutkiewicz, A., & Eadington, P. J. (2001). Assessing the maturity of oil trapped in fluid inclusions using molecular geochemistry data and visually-determined fluorescence colours. *Applied Geochemistry*, *16*, 451–473.

Goldstein, R. H., & Reynolds, T. J. (1994). Systematics of fluid inclusions in diagenetic minerals. *Society for Sedimentary Geology Short Course*, *31*, 199.

Greenwood, P. F., George, S. C., & Hall, K. (1998). Applications of laser micropyrolysis-gas chromatography–mass spectrometry. *Inorganic Chemistry*, *37*, 6288–6294.

Guilhaumou, N., Szydlowskii, N., & Pradier, B. (1990). Characterization of hydrocarbon fluid inclusions by infra-red and fluorescence microscopy. *Mineralogical Magazine*, *54*, 311–324.

Guilhaumou, N., Touray, J. C., & Bouhlel, S. (1988). Stretching behaviour of oil inclusions in fluorite under elevated confined pressure (200, 400) bar. Application to low pressure geobarometry. *Bulletin Minéralogique*, *111*, 421–426.

Horsfield, B., & McLimans, R. K. (1984). Geothermometry and geochemistry of aqueous and oil-bearing fluid inclusions from Fateh Field, Dubai. *Organic Geochemistry*, *6*, 733–740.

Isaksen, G., Pottorf, R., & Jenssen, A. I. (1998). Correlation of fluid inclusions and reservoired oils to infer trap fill history in the South Viking Graben, North Sea. *Petroleum Geoscience*, *4*, 41–55.

Jensenius, J., & Burruss, R. C. (1990). Hydrocarbon–water interactions during brine migration: Evidence from hydrocarbon inclusions in calcite cements from Danish North Sea oil fields. *Geochimica et Cosmochimica Acta*, *54*, 705–714.

Karlsen, D., Nedkvitne, T., Larter, S. R., & Bjørlykke, K. (1993). Hydrocarbon composition of authigenic inclusions: Applications to elucidation of petroleum reservoir filling history. *Geochimica et Cosmochimica Acta*, *57*, 3641–3659.

Kihle, J. (1996). Adaptation of fluorescence excitation-emission microspectroscopy for characterization of single hydrocarbon fluid inclusions. *Organic Geochemistry*, *23*, 1029–1042.

Kissin, Y. V. (1987). Catagenesis and composition of petroleum: Origin of *n*-alkanes and isoalkanes in petroleum crudes. *Geochimica et Cosmoschimica Acta*, *51*, 2445–2457.

Larter, S., & Mills, N. (1990). Phase-controlled molecular fractionations in migrating petroleum charges. In W.A. England, A.J. Fleet (Eds.), *Geological Society Special Publication*, *59*, 137–147.

McAuliffe, C. D. (1979). Oil and gas migration: Chemical and physical constraints. *American Association of Petroleum Geologists Bulletin*, *63*(5), 761–778.

Mcleod, G., Larter, S. R., Aplin, A. C., Pedersen, K. S., Booth, T. A. (1996). Determination of the effective composition of single petroleum inclusions using Confocal Scanning Laser Microscopy and PVT simulation. In P. E. Brown, S. G. Hagemann (Eds.), *Biennial Pan-American Conference on Research on Fluid Inclusions (PACROFI VI)* (pp. 81–82), Madison, WI.

Meulbroek, P., Cathles, L., & Whelan, J. (1998). Phase fractionation at South Eugene Island Block 330. *Organic Geochemistry*, *29*, 223–239.

Montel, F. (1993). Phase equilibria needs for petroleum exploration and production industry. *Fluid Phase Equilibria*, *84*, 343–367.

Munz, I. A., Johansen, H., Holm, K., & Lacharpagne, J.-C. (1999). The petroleum characteristics and filling history of the Frøy field and the Rind Discovery, Norwegian North Sea. *Marine and Petroleum Geology*, *16*, 633–651.

Murray, R. C. (1957). Hydrocarbon fluid inclusions in quartz. *American Association of Petroleum Geologists Bulletin*, *41*, 950–956.

Narr, W., & Burruss, R. (1984). Origin of reservoir fractures in Little Knife Field, North Dakota. *American Association Petroleum Geologists Bulletin*, *68*, 1087–1100.

Nichita, D. V., Minescu, F., & Cretu, I. (2001). Regression analysis and C7 + description for accurate PVT data calculations with equations of state. *Petroleum Geoscience*, *7*(2), 181–190.

Pagel, M., Walgenwitz, F., & Dubessy, J. (1986). Fluid inclusions in oil and gas-bearing sedimentary formations. In J. Burrus (Ed.), *Thermal Modeling in Sedimentary Basins*. Paris: Editions Technip.

Pang, L. S. K., George, S. C., & Quezada, R. A. (1998). A study of the gross composition of oil-bearing fluid inclusions using high performance liquid chromatography. *Organic Geochemistry*, *29*, 1149–1161.

Peng, D. Y., & Robinson, D. B. (1976). A new two-constant equation of state. *Industrial Engineering Chemicals Fundamentals*, *15*, 59–64.

Pironon, J., & Barrès, O. (1990). Semi-quantitative FT-IR microscopy limits: Evidence from synthetic hydrocarbon fluid inclusions in sylvite. *Geochimica et Cosmochimica Acta*, *54*, 509–518.

Pironon, J., & Barrès, O. (1992). Influence of brine–hydrocarbon reactions on FT-IR microspectroscopic analysis of intracrystalline liquid inclusions. *Geochimica et Cosmochimica Acta*, *56*, 169–174.

Pironon, J., Canals, M., Dubessy, J., Walgenwitz, F., & Laplace-Builhe, C. (1998). Volumetric reconstruction of individual oil inclusions by confocal scanning laser microscopy. *European Journal of Mineralogy*, *10*, 1143–1150.

Pironon, R., Thiéry, R., Teinturier, S., & Walgenwitz, F. (2000). Water in petroleum inclusions: Evidence from Raman and FT-IR measurements, PVT, consequences. *Journal of Geochemical Exploration*, *69/70*, 663–668.

Roedder, E. (1984). Fluid inclusions. In P. H. Ribbe (Ed.), (*Vol. 12*) (pp. 646) *Reviews in Mineralogy*, Mineralogical Society of America.

Silverman, S. R. (1963). Migration and segregation of oil and gas. *American Association of Petroleum Geologists Bulletin*, *47*(12), 2075–2076.

Thompson, K. F. M. (1987). Fractionated aromatic petroleums and the generation of gas-condensates. *Organic Geochemistry*, *11*(6), 573–590.

Thompson, K. F. M. (1988). Gas-condensate migration and oil fractionation in deltaic systems. *Marine and Petroleum Geology*, *5*, 237–246.

VTFlinc (1997). *User's guide*. Lingby, Denmark: CALSEP A/S, Chemical Engineering Consulting.